

SEMI-CLASSICAL THEORY OF MAGNETORESISTANCE ANOMALIES IN BALLISTIC MULTI-PROBE CONDUCTORS

C.W.J. Beenakker and H. van Houten

Philips Research Laboratories
5600 JA Eindhoven
The Netherlands

1. INTRODUCTION

The regime of ballistic transport in a two-dimensional electron gas (2DEG) was opened up a few years ago, when it became possible technically to reduce the dimensions of a conductor to below a mean free path. In this regime the resistance is determined by the geometry of the conductor, to the extent that impurity scattering can be neglected. In the usual regime of diffusive transport, the Hall bar geometry (a straight current-carrying channel with small side contacts for voltage drop measurements) is most convenient to determine the various components of the resistivity tensor separately. A down-scaled Hall bar was therefore the natural first choice as a geometry to study ballistic transport in a 2DEG (Timp et al., 1987; Roukes et al., 1987; Takagaki et al., 1988; Simmons et al., 1988; Chang et al., 1988; Ford et al., 1988). The point contact geometry (a short and narrow constriction) was an alternative choice (Van Wees et al., 1988; Wharam et al., 1988; Van Houten et al., 1988a). As it turns out, it is much easier to understand ballistic transport through a point contact than through a narrow Hall bar. The reason is that the resistance of a point contact is determined mainly by the number of occupied 1-dimensional subbands at the narrowest point of the constriction, and not so much by its shape (cf. the very similar results of Van Wees et al. (1988) and Wharam et al. (1988) on the quantized resistance of point contacts of a rather different design). The resistances measured in a narrow channel geometry, in contrast, are mainly determined by scattering at the junction with the side probes (Timp et al., 1988), which is different for junctions of different shape. The strong dependence of the low-field Hall resistance on the junction shape was demonstrated theoretically by Baranger and Stone (1989), and experimentally by Ford et al. (1989a) and Chang et al. (1989). These results superseded many earlier attempts (including one of our own) to explain the discovery by Roukes et al. (1987) of the *quenching of the Hall effect* without modelling the shape of the junction realistically (Beenakker and Van Houten, 1988; Peeters, 1988; Phillips, 1988; Akera and Ando, 1989; Srivastava, 1989; Johnston and Schweitzer, 1989; Isawa, 1989). Baranger and Stone (1989) argued that the rounded corners (present in a realistic situation) at the junction between the main channel and the side branches lead to a suppression (quenching) of the Hall resistance at low magnetic fields as a consequence of the *horn collimation effect* (an effect first proposed in the context of the point contact geometry (Beenakker and Van Houten, 1989a)). A Hall bar with straight corners, in contrast, does not show a generic suppression of the Hall resistance (Ravenshall et al., 1989; Kirczenow, 1989a), although quenching can occur for special parameter values if only a few subbands are occupied in the channel.

The quenched Hall effect (Roukes et al., 1987; Ford et al., 1988; 1989a; Chang et al., 1989) is just one of a whole variety of magnetoresistance anomalies observed in narrow Hall bars. Other anomalies are: the *last Hall plateau* (Roukes et al., 1987; Timp et al., 1987; Simmons et al., 1988; Ford et al., 1988; 1989a; Chang et al., 1988; 1989), reminiscent of quantum Hall plateaus, but occurring at much lower fields; the *negative Hall resistance* (Ford et al., 1989a), as if the carriers were holes rather than electrons; the *bend resistance* (Takagaki et al., 1988; 1989a; 1989b; Timp et al., 1988; 1989), a longitudinal resistance associated with a current bend, which is negative at small magnetic fields and zero at large fields, with an overshoot to a positive value at intermediate fields; and more.

In a recent paper (Beenakker and Van Houten, 1989b) we have shown that, at least qualitatively, all these phenomena can be explained in terms of a few simple semi-classical mechanisms. Since the magnetoresistance anomalies could be reproduced by a numerical simulation of the trajectories of electrons at the Fermi energy, it could be concluded that these are essentially classical rather than quantum size effects. In the present paper several aspects of our theory of junction scattering are discussed in more detail. In addition we present a direct comparison between the simulation and representative experiments, in order to determine to what extent a quantitative description of the magnetoresistance anomalies can be obtained with a semi-classical model in which quantum interference effects and lateral quantisation are not taken into account.

The outline of this paper is as follows. In Sec. 2 the classical mechanisms responsible for the magnetoresistance anomalies are presented. Our method of simulation is described in Sec. 3, and the results are compared with experiment in Sec. 4. We conclude in Sec. 5 with a critical discussion of the merits and limitations of our approach, and of the various alternative mechanisms proposed for the quenching of the Hall effect. In that section we also describe the modification of electron focusing in a narrow channel geometry and discuss the possible role of chaos in ballistic transport.

2. MECHANISMS

The variety of magnetoresistance anomalies mentioned above can be understood in terms of a few simple characteristics of the curved trajectories in a classical billiard in the presence of a perpendicular magnetic field (Beenakker and Van Houten, 1989b). At very small magnetic fields, *collimation* and *scrambling* are the key concepts. The gradual widening of the channel on approaching the junction reduces the injection/acceptance cone, which is the cone of angles with the channel axis within which an electron is injected into the junction, or within which an electron can enter the channel coming from the junction. This is the horn collimation effect (Beenakker and Van Houten, 1989a). An experimental demonstration of this effect using two opposite point contacts as injector and collector of the collimated beam has been given by Molenkamp et al. (1989). If the injection/acceptance cone is smaller than 90° , then the cones of two channels at right angles do not overlap. That means that an electron approaching the side probe coming from the main channel will be reflected (Fig. 1a), and will then typically undergo multiple reflections in the junction region (Fig. 1b). The trajectory is thus scrambled, whereby the probability for the electron to enter the left or right side probe in a weak magnetic field is equalized. This suppresses the Hall voltage. Our "scrambling" mechanism for the quenching of the Hall effect requires a weaker collimation than the "nozzle" mechanism put forward by Baranger and Stone (1989) (we return to both these mechanisms in Sec. 5). Scrambling is not effective in the geometry shown in Fig. 1c, in which a large portion of the boundary in the junction is oriented at approximately 45° with the channel axis. An electron reflected from a side probe at this boundary has a large probability of entering the opposite side probe. This is the "rebound" mechanism for a negative Hall resistance proposed by Ford et al. (1989a).

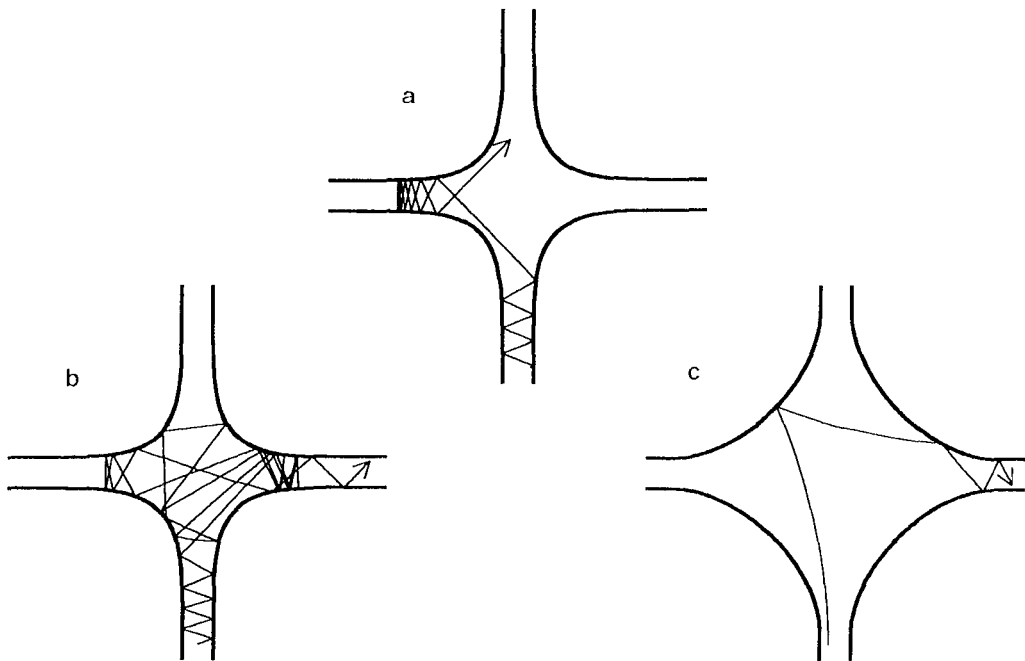


Fig. 1. Classical trajectories in an electron billiard, illustrating the collimation (a), scrambling (b), and rebound (c) effects.

At somewhat larger magnetic fields, *guiding* takes over. As illustrated in Fig. 2a, the electron is guided by the magnetic field along equipotentials around the corner. Guiding is fully effective when the cyclotron radius $l_{\text{cycl}} \equiv \hbar k_{\text{F}} / eB$ (with k_{F} the Fermi wave vector) becomes smaller than the minimal radius of curvature r_{min} of the corner, that is for magnetic fields greater than the guiding field $B_{\text{g}} \equiv \hbar k_{\text{F}} / e r_{\text{min}}$. In the regime $B \gtrsim B_{\text{g}}$ the junction can not scatter the electron back into the channel from which it came. The absence of backscattering is characteristic for the quantum Hall effect regime (Büttiker, 1988), but is in this case an entirely classical, weak-field phenomenon (Van Houten et al., 1988b). Because of the absence of backscattering, the longitudinal resistance vanishes, and the Hall resistance R_{H} becomes equal to the contact resistance of the channel, just as in the quantum Hall effect – but without quantisation of R_{H} . The contact resistance $R_{\text{contact}} \approx (h/2e^2) (\pi/k_{\text{F}} W)$ is approximately independent of the magnetic field for fields such that the cyclotron diameter $2l_{\text{cycl}}$ is greater than the channel width W , that is for fields below $B_{\text{crit}} \equiv 2\hbar k_{\text{F}} / eW$ (Van Houten et al., 1989). This explains the occurrence of the so-called “last plateau” in R_{H} for $B_{\text{g}} \lesssim B \lesssim B_{\text{crit}}$ as a classical effect. At the low-field end of the plateau, the Hall resistance is sensitive to *geometrical resonances* which increase the fraction of electrons guided around the corner into the side probe Fig. 2b illustrates the occurrence of such a geometrical resonance as a result of the magnetic focusing of electrons into the side probe, at magnetic fields such that the separation D of the two perpendicular channels (measured along the junction boundary, see Fig. 2b) is an integer multiple of the cyclotron diameter. This is in direct analogy with electron focusing in a double point contact geometry (Van Houten et al., 1988a; 1989). As shown in Fig. 3, electron focusing thus leads to periodic oscillations superimposed on the Hall plateau with maxima at approximately integer multiples of the focusing field $B_{\text{focus}} \equiv 2\hbar k_{\text{F}} / eD$ (indicated by arrows). In this geometry the oscillations become very large because the boundary at the junction has no curvature.

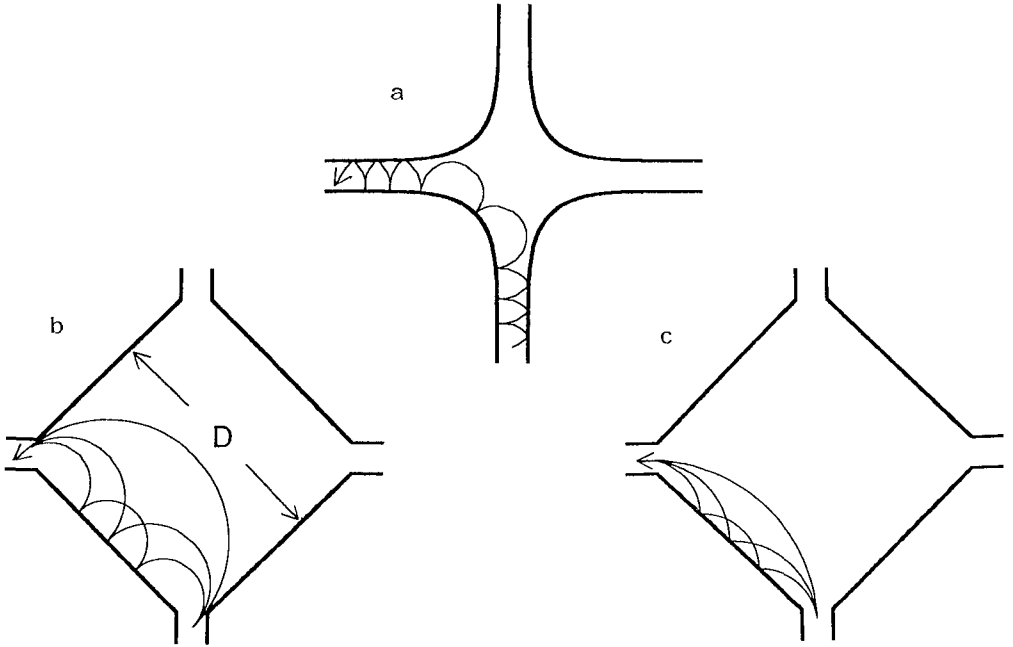


Fig. 2. Illustration of the guiding effect (a), and of two mechanisms leading to geometrical resonances (b,c). In (b) the trajectories are shown at three multiples of the focusing field B_{focus} , in (c) at three multiples of $B_{\text{focus}}/\sqrt{2}$.

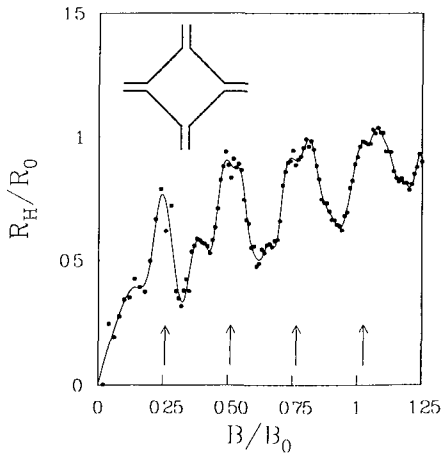


Fig. 3. Hall resistance in the hard-wall geometry shown in the inset. The curve drawn through the calculated data points is a guide to the eye. The arrows indicate magnetic fields at multiples of $B_{\text{focus}} \equiv (2W/D) B_0$ at which electron focusing in the junction occurs (cf. Fig. 2b). The parameters B_0 and R_0 are defined in Eq. (5).

Electron focusing in a Hall cross requires that electrons can be injected into the junction at 90° with the side wall connecting the injection probe with the side probe. The collimation effect, however, favors injection at 45° with this boundary, and thus may suppress electron focusing in favor of another geometrical resonance, illustrated in Fig. 2c. A collimated beam is bent by the magnetic field into the side probe (without focusing) when D is an integer multiple of the chord length $2l_{\text{cycl}}/\sqrt{2}$ of the electrons in the beam. This leads to oscillations in R_{II} with periodicity $B_{\text{focus}}/\sqrt{2}$. In Fig. 3 these more rapid oscillations are not clearly visible because of the absence of appreciable collimation in this particular geometry. In realistically smooth geometries both mechanisms discussed above, as well as additional geometrical resonances, may play a role. Note that these mechanisms for oscillations in the resistance depend on a commensurability between the cyclotron radius and a characteristic dimension of the junction, but do not involve the wave length of the electrons as an independent length scale. This distinguishes these geometrical resonances conceptually from the quantum resonances due to bound states in the junction considered by others (Avishai and Band, 1989; Ravenhall et al., 1989; Kirczenow, 1989a; 1989b; Peeters, 1989).

3. MODEL

To calculate the resistances in the semi-classical limit we use the Landauer-Büttiker formalism (Landauer, 1957; Büttiker, 1986), by which the resistances can be expressed as rational functions of transmission probabilities for electrons with the Fermi energy. The central equations, in a form suitable for a semi-classical calculation, are

$$I_i = G_i(1 - t_{i \rightarrow i})V_i - \sum_{j \neq i} G_j t_{j \rightarrow i} V_j, \quad (1)$$

where I_i is the current in channel i , eV_i is the chemical potential of a reservoir in equilibrium connected to channel i , $G_i \equiv (2e^2/h)N_i$ is the contact conductance of channel i , and $t_{j \rightarrow i}$ is the fraction of the current injected into channel j which leaves the system via channel i . The number N_i in the definition of the contact conductance is the number of transverse waveguide modes at the Fermi energy in channel i . In the semi-classical limit, N is treated as a continuous variable, e.g. at zero magnetic field $N \equiv k_1 W/\pi$ for a channel defined by a square well confining potential with width W . The transmission probabilities in a magnetic field B satisfy the symmetry relation (Büttiker, 1986)

$$G_j(B) t_{j \rightarrow i}(B) = G_i(B) t_{i \rightarrow j}(-B), \quad (2)$$

(note that G is symmetric in B), and obey the normalization

$$\sum_j t_{i \rightarrow j} = 1. \quad (3)$$

Eqs. (2) and (3) together imply that

$$\sum_j G_j t_{j \rightarrow i} = G_i. \quad (4)$$

Once the coefficients in Eq. (1) are known, the voltages V_i can be obtained by solving the set of linear equations for given currents I_i . The four-terminal resistances are defined as $R_{ij,kl} \equiv (V_k - V_l)/I_i$, where $I_i = -I_j \equiv I$ and $I_m = 0$ for $m \neq i, j$.

The algorithm used to calculate the coefficients in Eq. (1) is straightforward, except for one point (the injection distribution). We simulate the injection of a large number (from 10^3 to 4×10^4 , depending on the accuracy required) of electrons towards

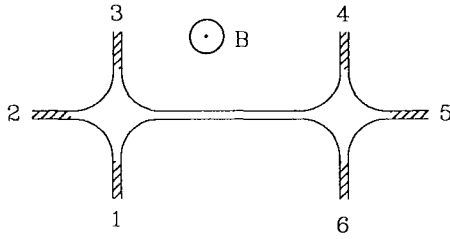


Fig. 4. Double junction geometry, with the hard-wall, field-free leads shown shaded.

the junction through channel j , and integrate Newton's equations of motion numerically to determine the fraction $t_{j \rightarrow i}$ of electrons leaving the junction via channel i . The injection distribution has to be chosen such that the current injected in the channel is uniformly distributed among the modes, to simulate injection by a reservoir in thermal equilibrium. In a hard-wall channel (defined by a square well confining potential), in zero magnetic field, this is realized by injecting the electrons uniformly over the channel width W , with Fermi velocity v_F , and angular distribution $P(\alpha) = (\cos \alpha)/2$ (α in the interval $(-\pi/2, \pi/2)$ being the angle with the channel axis). The contact conductance is then given by $G = (2e^2/h)(k_F W/\pi)$, and all coefficients in Eq. (1) can be obtained. For other confining potentials, or for $B \neq 0$, both the injection distribution and the contact conductances are different, and not easily calculated. We circumvent this difficulty by attaching to each channel of the structure a hard-wall lead in which $B = 0$ (shaded in Fig. 4). This trick does not change the resistances in the semi-classical limit (see below), while it permits us to use the simple expressions for $P(\alpha)$ and G given above.

It remains to prove the correctness of the injection trick. Consider attaching to channel i a hard-wall, field-free lead (one of the shaded leads in Fig. 4). First note that trajectories which leave the junction through channel i are not reflected at the interface with the shaded lead. Moreover, if the shaded lead is attached at more than a few channel widths from the junction it has no influence on the dynamics in the junction itself. The transmission probabilities $t_{j \rightarrow j}$ and $t_{j \rightarrow i}$ for $j \neq i$ are therefore unaffected. The contact conductances G_j for $j \neq i$ are also unchanged, of course. This holds for all B , so that in view of the symmetry relation (2) the product $G_i t_{i \rightarrow j}$ for $j \neq i$ is unchanged as well. Finally, also the term $G_i(1 - t_{i \rightarrow i})$ remains the same, since by virtue of Eq. (4) this quantity is given by

$$G_i(1 - t_{i \rightarrow i}) = \sum_{j \neq i} G_j t_{j \rightarrow i}.$$

All the coefficients in Eq. (1), which determines the resistances, are therefore the same as they were before the shaded lead was attached to channel i . We can now repeat the argument and attach a hard-wall, field-free lead to each of the channels without any effect on the resistances. Note that this injection trick is correct in the semi-classical limit only. In the quantum-mechanical problem, spurious reflections will occur on approaching the shaded lead from the unshaded part of the channel. These may be eliminated by a gradual (adiabatic) transition to a hard-wall, field-free lead (Baranger and Stone, 1989). By our method the properties of the reservoirs, on which the Landauer-Büttiker formalism is based, are taken into account properly. For a discussion of the extent to which actual ohmic contacts approximate the theoretical reservoirs, see e.g. the paper by Komiyama and Hirai (1989).

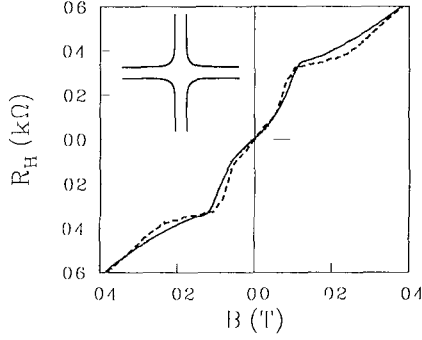


Fig. 5. Hall resistance as measured (solid curve) by Simmons et al. (1988), and as calculated (dashed curve) for the hard-wall geometry in the inset ($W = 0.8 \mu\text{m}$ and $E_F = 14 \text{ meV}$). The dotted line is R_{II} in a bulk 2DEG.

4. THEORY VERSUS EXPERIMENT

An overview of the magnetoresistance anomalies exhibited by the semi-classical theory has been given in our earlier paper (Beenakker and Van Houten, 1989b). Here we present a direct comparison between theory and representative experiments on laterally confined two-dimensional electron gases in high-mobility GaAs-AlGaAs heterostructures. In the calculation we chose a parabolic confining potential for the narrowest channels (of width around 100 nm), and a square well confining potential for wider channels. In the junction the equipotentials are segments of the curve $|x|^p + |y|^p = \text{constant}$, with the power $p > 1$ parameterizing the smoothness of the corners (the larger p , the sharper the corners). We first discuss the Hall resistance R_{II} .

Fig. 5 shows the precursor of the classical Hall plateau (the "last plateau") in a relatively wide Hall cross. The experimental data* (solid curve) is from a paper by Simmons et al. (1988). Our calculation (dashed curve) is for a square well confining potential of channel width $W = 0.8 \mu\text{m}$ (as estimated in the experimental paper), and with the relatively sharp corners shown in the inset (corresponding to $p = 8$, $r_{\text{min}} \approx 0.8W$). The Fermi energy used in the calculation is $E_F = 14 \text{ meV}$, which corresponds (via $n_s = E_F / m / \pi \hbar^2$) to a sheet density in the channel of $n_s = 3.9 \times 10^{15} \text{ m}^{-2}$, somewhat below the value of $4.9 \times 10^{15} \text{ m}^{-2}$ of the bulk material in the experiment. Good agreement between theory and experiment is seen in Fig. 5. Near zero magnetic field, the Hall resistance in this geometry is close to the linear result $R_{\text{II}} = B / en_s$ for a bulk 2DEG (dotted line). The corners are sufficiently smooth to generate a Hall

*The experimental curves in Figs. 5 and 7 are (anti-)symmetrized resistances,

$$R_{ij,kl}^{\Lambda} = \frac{1}{2} [R_{ij,kl}(B) - R_{kl,ij}(-B)], \quad R_{ij,kl}^{\text{S}} = \frac{1}{2} [R_{ij,kl}(B) + R_{kl,ij}(-B)].$$

reported in this way in many of the experimental papers.

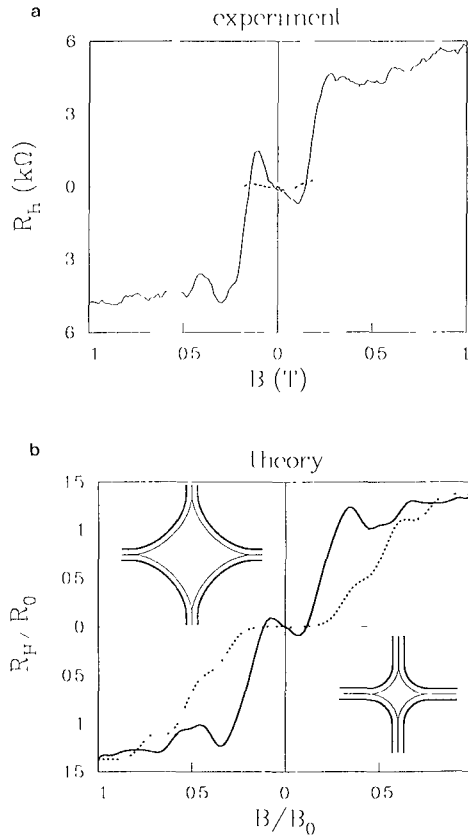


Fig. 6. Hall resistance as measured (a) by Ford et al. (1989a), and as calculated (b). In (a) as well as in (b), the solid curve corresponds to the geometry in the upper left inset, and the dotted curve to the geometry in the lower right inset. The insets in (a) indicate the shape of the gates, not the actual confining potential. The insets in (b) show equipotentials of the confining potential at E_F (thick contour) and 0 (thin contour). The potential rises parabolically from 0 to E_F , and vanishes in the diamond-shaped region at the center of the junction.

plateau[†] via the guiding mechanism discussed in Sec. 2. The horn collimation effect, however, is not sufficiently large to suppress R_{II} at small B . Indeed, the injection/acceptance cone for this junction is considerably wider than the maximal angular opening of 90° required for quenching of the Hall effect via the scrambling mechanism of Sec. 2 (see the angular injection distribution given in Fig. 3, dashed curve, of our earlier paper (Beenakker and Van Houten, 1989b), which shows an injection/acceptance cone of about 115° for this geometry).

The low-field Hall resistance changes drastically if the channel width becomes smaller, relative to the radius of curvature of the corners. Fig. 6a shows experimental data by Ford et al. (1989a). The solid and dotted curves are for the geometries shown respectively in the upper left and lower right insets of Fig. 6a. Note that these insets indicate the gates with which the Hall crosses are defined electrostatically. The equipotentials in the 2DEG will be smoother than the contours of the gates. The experiment shows a well developed Hall plateau, with superimposed fine structure. At small positive fields R_{II} is either quenched or negative, depending on the geometry. The geometry is seen to affect also the width of the Hall plateau – but not the height. In Fig. 6b we give our numerical results for the two geometries in the insets, which we believe to be reasonable representations of the confining potential induced by the gates in the experiment (although no attempt was made to actually solve the electrostatic problem). We used a parabolic confining potential in the channel and equipotentials at the corners defined by $p=1.7$ and $p=2$ in the upper left and lower right inset, respectively*. In the theoretical plot the resistance and the magnetic field are given in units of

$$R_0 \equiv \frac{h}{2e^2} \frac{\pi}{k_F W}, \quad B_0 \equiv \frac{\hbar k_F}{eW}, \quad (5)$$

where the channel width W for the parabolic confinement is defined as the separation of the equipotentials at the Fermi energy. The experimental estimates $W \approx 90$ nm, $n_s \approx 1.2 \times 10^{15} \text{ m}^{-2}$ imply $R_0 = 5.2$ k Ω , $B_0 = 0.64$ T. With these parameters the calculated resistance and field scales do not agree well with the experiment, which may be due in part to the uncertainties in our modelling of the shape of the experimental confining potential. The $\pm B$ asymmetry in the experimental plot is undoubtedly due to asymmetries in the cross geometry (in the calculation the geometry has four-fold symmetry, which leads automatically to $R_{II}(B) = -R_{II}(-B)$). Apart from these differences, there is agreement in all the important features: the appearance of quenched and negative Hall resistances, the independence of the height of the last Hall plateau on the smoothness of the corners, and the shift of the onset of the last plateau to lower fields for smoother corners. The oscillations on the last plateau in the calculation (which as we discussed in Sec. 2 are due to geometrical resonances) are also quite similar to those in the experiment, in support of our claim that these are classical rather than quantum resonances.

[†]In this junction with a rapidly varying curvature, the guiding field $B_g \approx 0.16$ T of Sec. 2 is somewhat too large an estimate of the low-field onset of the Hall plateau. The upper limit of the plateau is accurately given by $B_{\text{crit}} \approx 0.26$ T.

*The geometry in the lower right inset (with an approximately constant curvature of the corners) has $r_{\text{min}} = 2W$. The resulting guiding field $B_g = 0.5B_0$ is seen to correspond accurately to the low-field onset of the Hall plateau (cf. the dashed curve in Fig. 6b). The angular opening of the injection/acceptance cone in this case is below 90° , consistent with the appearance of a quenched R_{II} in the calculation.

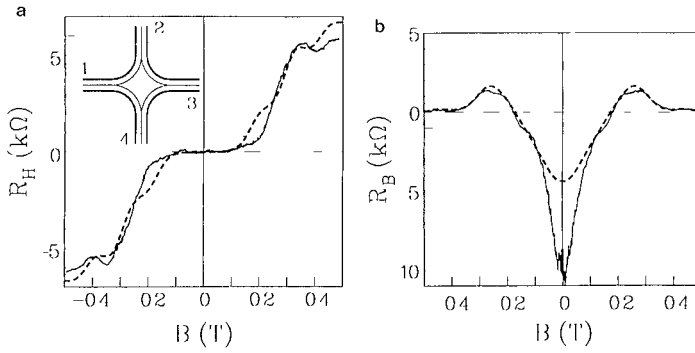


Fig. 7. Hall resistance $R_{\text{H}} \equiv R_{13,24}$ (a) and bend resistance $R_{\text{B}} \equiv R_{12,43}$ (b), as measured (solid curves) by Timp et al. (1989), and as calculated (dashed curves) for the geometry in the inset (consisting of a parabolic confining potential with the equipotentials at E_{F} and 0 shown respectively as thick and thin contours; the parameters are $W = 100$ nm and $E_{\text{F}} = 3.9$ meV). The dotted line in (a) is R_{H} in a bulk 2DEG.

We now turn to the bend resistance R_{B} . In Fig. 7 we show experimental data[†] by Timp et al. (1989) (solid curves) on $R_{\text{B}} \equiv R_{12,43}$ and $R_{\text{H}} \equiv R_{13,24}$ measured in the same Hall cross (defined by gates of a shape similar to that in the lower right inset of Fig. 6a; see the inset of Fig. 7a for the numbering of the channels). The dashed curves are calculated for a parabolic confining potential in the channels (with the experimental values $W = 100$ nm, $E_{\text{F}} = 3.9$ meV), and with corners as shown in the inset of Fig. 7a (defined by $p = 2$). The calculated quenching of the Hall resistance and the onset of the last plateau are in good agreement with the experiment, and also the observed overshoot of the bend resistance around 0.2 T as well as the width of the negative peak in R_{B} around zero field are well described by the calculation. The calculated height of the negative peak, however, is too small by more than a factor of two. We consider this disagreement to be significant in view of the quantitative agreement with the other features in both R_{B} and R_{H} . The negative peak in R_{B} is due to the fact that the collimation effect couples the current source 1 more strongly to voltage probe 3 than to voltage probe 4, so that $R_{\text{B}} \propto V_4 - V_3$ is negative for small magnetic fields (at larger fields the Lorentz force destroys collimation by bending the trajectories, so that R_{B} shoots up to a positive value*, until guiding takes over and brings R_{B} down to zero by eliminating backscattering at the junction). The discrepancy in Fig. 7b thus seems to indicate that the semi-classical calculation underestimates the collimation effect in this geometry.

As we showed earlier (Beenakker and Van Houten, 1989b), the positive resistance peak in the bend resistance coincides in magnetic field range with a peak of enhanced longitudinal resistance R_{L} measured along the current-carrying channel ($R_{\text{L}} \equiv R_{25,34}$ in the geometry of Fig. 4). The peak in the longitudinal resistance has the same origin as in the case of the bend resistance discussed above, viz. the destruction of the collimation effect by the magnetic field. A collimated beam propagating along the channel will not be scattered very much by the side branches, and thus corresponds to a low R_{L} . A weak

[†]The (anti-)symmetrized resistances are plotted in Fig. 7.

*We only find the positive overshoot in R_{B} for rounded corners. This explains the near absence of the effect in the calculation of Kirczenow (1989b) for a junction with straight corners.

magnetic field destroys the collimation effect, thereby increasing the backscattering by the side branches and thus increasing R_{\perp} . Magnetic guiding at larger fields reduces R_{\perp} , so that our calculations show a "camel-back" B -dependence. Backscattering by channel wall irregularities leads to a similar non-monotonic magnetoresistance, an effect discovered in sodium wires forty years ago by MacDonald (1949). This effect (not included in our calculations in which a smooth, straight channel is assumed) is actually the dominant mechanism for the camel-back magnetoresistance in the systems studied thus far, as has been demonstrated convincingly in a set of experiments by Thornton et al. (1989).

We conclude this section with a discussion of the temperature dependence of the magnetoresistance anomalies. The theoretical results in Figs. 5-7 are for $T = 0$. The resistance $R(T, E_{\text{F}})$ at temperature T and chemical potential E_{F} follows from Eq. (1) with thermally averaged coefficients

$$I_i = \langle G_i(1 - t_{i \rightarrow i}) \rangle V_i - \sum_{j \neq i} \langle G_j t_{j \rightarrow i} \rangle V_j, \quad (6)$$

Here $\langle \dots \rangle$ denotes the thermal average

$$\langle G t \rangle \equiv \int dE G(E) t(E) \frac{d}{dE_{\text{F}}} f(E - E_{\text{F}}), \quad (7)$$

where f is the Fermi function

$$f(E - E_{\text{F}}) = \left(1 + \exp \frac{E - E_{\text{F}}}{k_{\text{B}} T} \right)^{-1}. \quad (8)$$

The resistance R which follows from Eq. (6) is a rational function of the thermally averaged transmission probabilities. In a first approximation we can interchange the evaluation of the rational function and the average, and write $R(T, E_{\text{F}}) \approx \langle R(0, E_{\text{F}}) \rangle$. For $k_{\text{B}} T$ small compared to E_{F} , the thermal average can be approximated by the average of $R(0, E)$ over an energy interval $\Delta E = 3.5 k_{\text{B}} T$ around E_{F} (corresponding to the width of the derivative of the Fermi function). For the following considerations we assume a hard-wall confining potential, so that the geometry of the equipotentials is the same at each energy. (The conclusions hold also for a smooth potential, provided that the geometry does not change significantly if the energy of the equipotentials varies by ΔE around E_{F} .) For a fixed geometry, $R(0, E)$ depends on E only via the scaling variables R_0 and B_0 defined in Eq. (5), according to $R(0, E) \equiv R_0 \rho(\beta)$ with $\beta \equiv B/B_0$. The dimensionless resistance ρ is the quantity plotted e.g. in Fig. 6b. Since $d\beta/dE = -\beta/2E$ and R_0 are both only weakly dependent on E , the energy average of R over ΔE corresponds approximately to the magnetic field average of ρ over the interval $\Delta\beta = \Delta E \beta / 2E_{\text{F}}$. The finest details in our magnetoresistance plots (cf. Fig. 6b) occur for $\beta \lesssim 1$ and require a resolution $\Delta\beta \gtrsim 0.1$, so that at temperatures $T \sim 0.1 E_{\text{F}}/k_{\text{B}} \sim 10$ K these features are still resolved. Note that the energy separation of the subbands does not enter in our criterion for the temperature dependence, since the wave length is not an independent variable in the semi-classical theory.

The experiments shown above were carried out at temperatures around 1 K, for which we expect our zero-temperature semi-classical calculation to be appropriate. At lower temperatures the effects of quantum mechanical phase coherence which we have neglected will become more important (Ford et al., 1989b). At higher temperatures the thermal average smears out the magnetoresistance anomalies, and eventually inelastic scattering causes a transition to the diffusive transport regime in which the resistances have their normal B -dependence. Takagaki et al. (1989b) find that the bend resistance

is almost independent of temperature below 10 K, which is consistent with the above considerations.

5. CONCLUDING REMARKS

Merits and limitations

The overall agreement between the experiments and the semi-classical calculations demonstrated in this paper is remarkable in view of the fact that the channel width in the narrowest structures considered is comparable to the Fermi wave length. When the first experiments on these "electron waveguides" appeared, it was expected that the presence of only a small number of occupied transverse waveguide modes would fundamentally alter the nature of electron transport (Timp et al., 1987). Our results show instead that the modal structure plays only a minor role, and that the magnetoresistance anomalies observed are characteristic for the *classical* ballistic transport regime. The reason that a phenomenon such as the quenching of the Hall effect has been observed only in Hall crosses with narrow channels is simply that the radius of curvature of the corners at the junction is too small compared to the channel width in wider structures. This is not an essential limitation, and the various magnetoresistance anomalies discussed here should be observable in macroscopic Hall bars with artificially smoothed corners — provided of course that the dimensions of the junction remain well below the mean free path. Ballistic transport is essential, but a small number of occupied modes is not.

Although we believe that the characteristic features of the magnetoresistance anomalies are now understood, several interesting points of disagreement between theory and experiment remain which merit further investigation. One of these is the discrepancy in the magnitude of the negative bend resistance at zero magnetic field, which we discussed in Sec. 4. The disappearance of a region of quenched Hall resistance at low electron density is another unexpected observation by Chang et al. (1989) and Roukes et al. (1989). The semi-classical theory discussed in this paper predicts a universal behavior (for a given geometry) if the resistance and magnetic field are scaled by R_0 and B_0 defined in Eq. (5). For a square well confining potential the channel width W is the same at each energy, and since $B_0 \propto k_F$ one would expect the field region of quenched Hall resistance to vary with the electron density as $\sqrt{n_s}$. For a more realistic smooth confining potential, W depends on E_F and thus on n_s as well, in a way which is difficult to estimate reliably. In any case, the experiments point to a systematic disappearance of the quench at the lowest densities, which is not accounted for by the present theory (and has been attributed by Chang et al. (1989) to enhanced diffraction at low electron density as a result of the increase in the Fermi wave length). As a third point, we mention the curious density dependence of the quenching observed in approximately straight junctions by Roukes et al. (1989), who find a low-field suppression of R_{II} which occurs only at or near certain specific values of the electron density. Our semi-classical model applied to a straight Hall cross (either defined by a square well or by a parabolic confining potential) gives a low-field slope of R_{II} close to its bulk 2D value. The fully quantum mechanical calculations for a straight junction (Ravenhall et al., 1989; Kirczenow, 1989a) do give quenching at special parameter values, but not for the many-mode channels in this experiment (in which quenching occurs with as many as 10 modes occupied, whereas in the calculations a straight cross with more than 3 occupied modes in the channel does not show a quench).

In addition to the points of disagreement discussed above, there are fine details in the measured magnetoresistances, especially at the lowest temperatures (below 100 mK), which are not obtained in the semi-classical approximation. The quantum mechanical calculations (Ravenhall et al., 1989; Kirczenow, 1989a; 1989b; Baranger and Stone, 1989) show a great deal of fine structure due to interference of the waves scat-

tered by the junction. The fine structure in most experiments is not quite as pronounced as in the calculations, presumably partly as a result of a loss of phase coherence after many multiple scatterings in the junction (more than 10 boundary collisions in the junction before an electron escapes into one of the channels are common in our simulation, and it could well be that phase coherence is not maintained for the correspondingly long trapping times). The limited degree of phase coherence in the experiments, and the smoothing effect of a finite temperature, help to make the semi-classical model work so well even for the narrowest channels.

Some of the most pronounced features in the quantum mechanical calculations are due to transmission resonances which result from the presence of bound states in the junction (Avishai and Band, 1989; Ravenhall et al., 1989; Kirczenow, 1989a; 1989b; Peeters, 1989). In Sec. 2 of this paper we have emphasized a different mechanism for transmission resonances which has a classical rather than a quantum mechanical origin. As we have shown in Sec. 4, the oscillations on the last Hall plateau observed experimentally are quite well accounted for by these geometrical resonances. One way to distinguish experimentally between these resonance mechanisms is by means of the temperature dependence, which should be much weaker for the classical than for the quantum effect (cf. Sec. 4). One would thus conclude that the fluctuations in Fig. 6a, measured by Ford et al. (1989a) at 4.2 K, have a classical origin — while the fine structure which Ford et al. (1989b) observe only at mK temperatures is intrinsically quantum mechanical.

Routes to quenching

Among the magnetoresistance anomalies observed in the ballistic regime, the quenching of the Hall effect (Roukes et al., 1987) has the most subtle explanation, and is the most sensitive to the geometry. As we discussed in our earlier article (Beenakker and Van Houten, 1989b), and in Sec. 2 of the present paper, long trapping times in the junction play an essential role: the scrambling of the trajectories after multiple reflections suppresses the asymmetry between the transmission probabilities t_l and t_r to enter the left or right voltage probe, and without this transmission asymmetry there can be no Hall voltage. We emphasize that this *scrambling mechanism* is consistent with the original findings of Baranger and Stone (1989) that quenching requires collimation. The point is that the collimation effect leads to non-overlapping injection/acceptance cones of two perpendicular channels, which ensures that electrons can not enter the voltage probe from the current source directly — but only after multiple reflections (cf. Sec. 2). In this way a rather weak collimation to within an injection/acceptance cone of about 90° angular opening is sufficient to induce a suppression of the Hall resistance via the scrambling mechanism.

Collimation can also suppress R_{II} directly by strongly reducing t_l and t_r relative to t_s (the probability for transmission straight through the junction). This *nozzle mechanism*, introduced by Baranger and Stone (1989), requires a strong collimation of the injected beam in order to affect R_{II} appreciably. In the geometries considered here, we find that quenching of R_{II} is due predominantly to scrambling and not to the nozzle mechanism (t_l and t_r each remain more than 30% of t_s), but data by Baranger and Stone (1989) shows that both mechanisms can play an important role.

There is a third proposed mechanism for the quenching of the Hall effect (Ravenhall, 1989; Kirczenow, 1989a), which is the reduction of the transmission asymmetry due to a bound state in the junction. The *bound state mechanism* is purely quantum mechanical and does not require collimation (in contrast to the classical scrambling and nozzle mechanisms). Numerical calculations have shown that it is only effective in straight Hall crosses with very narrow channels (not more than 3 modes occupied), and even then for special values of the Fermi energy only. Although this mechanism can not account for the experiments performed thus far, it may become of

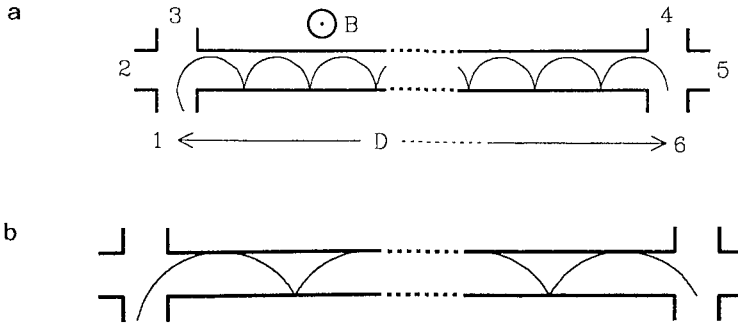


Fig. 8. Classical trajectories in a narrow channel, illustrating two types of geometrical resonances: electron focusing of skipping orbits (a), and quasi-electron focusing of traversing trajectories (b).

importance in future work. We note that while the bound state and the scrambling mechanism for quenching have a different origin, what unifies the two is that in both cases long trapping times in the junction are involved, suppressing R_{II} by eliminating the transmission asymmetry which the Lorentz force tries to impose. The nozzle mechanism, to the contrary, deals with trajectories which move straight through the junction with minimal time delay, so that it is distinct from the other two mechanisms in this respect.

Narrow-channel electron focusing

In Sec. 2 we showed how electron focusing in a junction (from current to voltage probe) can lead to large periodic oscillations in the Hall resistance in special geometries. In this paragraph we wish to describe a similar effect in a narrow channel. We consider the geometry shown in Fig. 8, defined by a hard-wall potential with *straight* rather than rounded corners. The resistance $R_{\Gamma} \equiv R_{12,65}$ is an example of what M.L. Roukes has termed a "transfer resistance" at this Conference. The net current flows entirely in one junction (from lead 1 to 2), while the voltage difference is measured between two side probes 6 and 5 in the other junction where no net current flows. Fig. 9 shows the result of our semi-classical calculation of R_{Γ} in this geometry. For one field direction R_{Γ} decreases smoothly with B , while for the other field direction a striking oscillatory pattern is superimposed.

The oscillations for $|B| > B_0$ are due to magnetic focusing of skipping orbits along the boundary from lead 1 to 6, as in the electron focusing experiment with point contacts in metals (Tsoi, 1974) or in a wide 2DEG (Van Houten et al., 1988a; 1989). The focusing periodicity is (cf. Sec. 2)

$$B_{\text{focus}} \equiv 2\hbar k_{\Gamma} / eD \equiv (2W/D) B_0, \quad (9)$$

which is $0.075 B_0$ for the center-to-center separation $D = 26.66 W$ of side branches 1 and 6 used in the calculation. This agrees well with the periodicity of the oscillations for $|B| > B_0$ in Fig. 9. The oscillations die out as $|B|$ approaches $B_{\text{crit}} \equiv 2B_0$, since the voltage difference $V_6 - V_5$ vanishes if the cyclotron diameter $2l_{\text{cycl}}$ becomes less than W (cf. Sec. 2).

Electron focusing is not possible for $|B| < B_0$, since skipping orbits with the maximum chord length $2l_{\text{cycl}}$ shown in Fig. 8a require a channel of width at least l_{cycl} to prevent collisions with the opposite channel wall. Collisions with both the channel

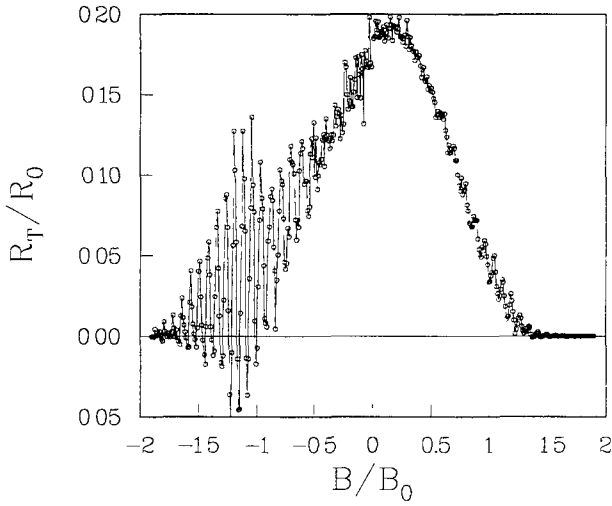


Fig. 9. Transfer resistance $R_{12,65}$ calculated for the hard-wall geometry of Fig. 8. The curve drawn through the data points is a guide to the eye.

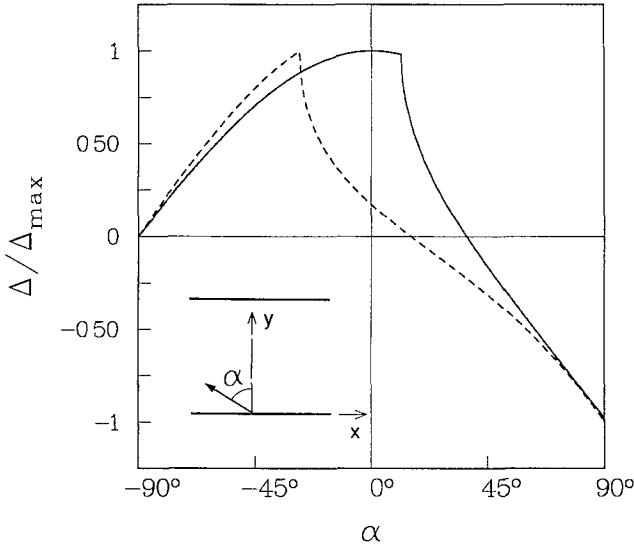


Fig. 10. Dependence on the injection angle α of the separation Δ between two subsequent collisions with the same boundary in the channel indicated in the inset ($\Delta > 0$ corresponds to motion in the positive x -direction). Results for two field values are plotted, corresponding to electron focusing (solid curve, $B = -1.2B_0$, as in Fig. 8a) and to quasi-electron focusing (dashed curve, $B = -0.53B_0$, as in Fig. 8b).

walls transform the skipping orbit into a traversing trajectory (Fig. 8b), and this destroys the focusing effect: a narrow flux tube containing traversing trajectories leaving probe 1 cannot be focused to a point at probe 6 by the magnetic field. Fig. 10 shows why: In this figure we have plotted for the two magnetic fields corresponding to Fig. 8a (solid curve, $B = -1.2B_0$) and 8b (dashed curve, $B = -0.53B_0$) the dependence on the injection angle α (indicated in the inset) of the distance Δ between two subsequent

collisions with the same channel boundary (Δ is normalized by its maximum Δ_{\max} as a function of α). For $|B| > B_0$ the curve $\Delta(\alpha)$ has a *smooth* maximum, while for $|B| < B_0$ the maximum is a *cusp*. In the former case Δ is stationary at Δ_{\max} for $\alpha \approx 0$, and thus the skipping orbits injected nearly perpendicular to the x -axis are focused at multiples of Δ_{\max} . There is no point of stationary Δ in the latter case, so that the traversing trajectories can not be focused.

Although focusing can not occur for $|B| < B_0$, one sees from Fig. 9 that oscillations in R_T persist almost down to zero field, albeit with decreasing amplitude and with a spacing ΔB which is not constant but is gradually reduced as $B \rightarrow 0$. We refer to these low-field oscillations in a narrow channel as *quasi-electron focusing*, since they result from a geometrical resonance involving traversing trajectories which is the analogue of focusing of skipping orbits in higher fields, or in wider channels. In both field regimes a peak in R_T occurs whenever $D = p\Delta_{\max}$, with p an integer. If $W > l_{\text{cycl}}$, then $\Delta_{\max} = 2l_{\text{cycl}}$ is the maximum chord length of a skipping orbit, and the above criterion is the usual electron focusing condition

$$|B| = pB_{\text{focus}}, \quad W > l_{\text{cycl}}. \quad (10)$$

If, on the other hand, $W < l_{\text{cycl}}$, then one has $\Delta_{\max} = 2W(2l_{\text{cycl}}/W - 1)^{1/2}$, so that one obtains the condition

$$|B| = pB_{\text{focus}} \frac{4pWD}{D^2 + (2pW)^2}, \quad W < l_{\text{cycl}}. \quad (11)$$

In agreement with the numerical results in Fig. 9, the oscillations in the resistance determined by Eq. (11) become more rapid at lower fields (corresponding to smaller values of the integer p), although the periodicity remains approximately equal to the focusing periodicity B_{focus} as long as W is not much smaller than l_{cycl} . The fields B_p defined in Eq. (11) are such that for $|B| < B_p$ electrons can be transmitted from probe 1 to probe 6 after $2p - 1$ specular reflections with the channel walls. The contribution of these trajectories to the transmission probability increases with B until at B_p this contribution drops abruptly to zero, leading to a sequence of oscillations in R_T . A similar effect in thin metal films has been discussed by Korzh (1975).

Chaotic scattering

The many multiple reflections in a junction with rounded corners lead to a strong sensitivity of the choice of exit channel (through which the electron leaves the junction) on the injection parameters. A plot of exit channel versus injection angle α shows an irregularly fluctuating "chaotic" behavior, as shown in Fig. 11a for zero magnetic field, and in Figs. 11b and c for $B = 0.2B_0$ and $B = B_0$ respectively. Chaotic scattering in similar geometries in the absence of a magnetic field has received considerable attention recently (Bleher et al., 1989; and references therein). We find that intervals in α of irregular dependence of the exit channel on the injection angle are separated by intervals in which one particular exit channel is favored. These "islands" of regular scattering grow with B , until for $B > B_{\text{crit}} \equiv 2B_0$ all electrons are guided into one particular channel (number 1 in the case of Fig. 11).

The chaotic behavior in Fig. 11 is a manifestation of the scrambling mechanism for the quenching of the Hall effect discussed above, but is not directly visible in the resistances considered thus far. The reason is that the average over the injection parameters which determines the transmission probabilities smears out most of the irregular fluctuations apparent in Fig. 11. A way in which one may be able to study the chaotic scattering in a resistance measurement is by measuring the voltage difference over a region through which no net current flows. The transfer resistance R_T considered above is such a quantity. In Fig. 12 we show our calculations of the B -dependence of R_T in the hard-wall geometry with rounded corners of Fig. 4. Because of the multiple

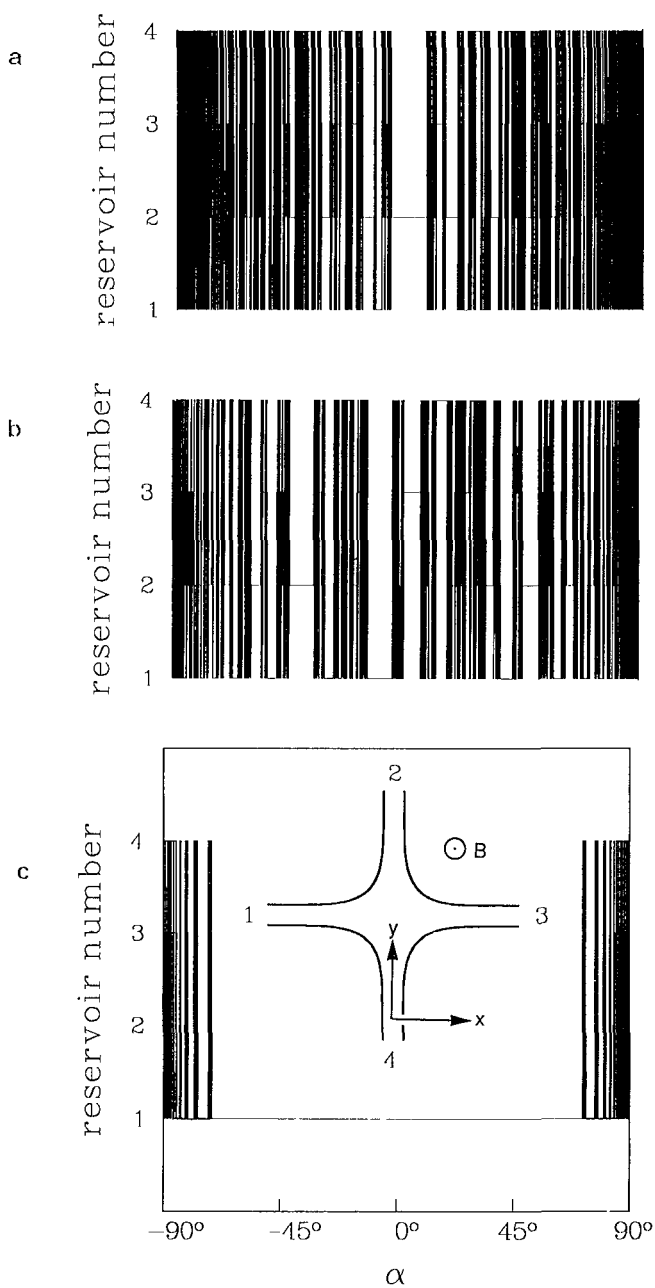


Fig. 11. Dependence of the choice of exit channel (numbered 1 through 4) on the injection angle, for $B = 0$ (a), $B = 0.2B_0$ (b), and $B = B_0$ (c). The electrons are injected into the junction shown in the inset, starting from the origin of the coordinate system at an angle α with the positive y - axis.

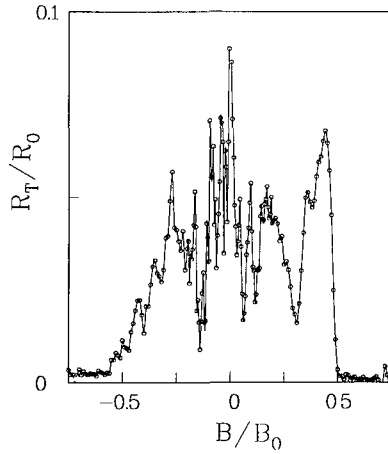


Fig. 12. Transfer resistance $R_{12,65}$ calculated for the hard-wall geometry of Fig. 4. The curve drawn through the data points is a guide to the eye.

scattering in the junction, R_T looks very different from the result in Fig. 9 for a junction with straight corners (in which multiple scattering is not possible). The (quasi-)electron focusing oscillations for negative B are not apparent in Fig. 12, but irregular fluctuations occur for both field directions. The fine details of these fluctuations are masked by numerical noise (which we estimate at $0.01 - 0.02R_0$ in these simulations, consisting of an average over 4×10^4 electrons). Voltage fluctuations in R_T have been observed by Takagaki et al. (1989a), who attributed them to a quantum interference effect. Our simulation shows that similar fluctuations can result from classical chaotic scattering.

Essentially, what we are doing in this simulation is to use one junction as an injector of ballistic electrons, and the other junction as a detector. Provided that the transport remains ballistic over the distance separating the two junctions (which may be difficult to realize experimentally because of the presence of a small amount of diffuse boundary scattering (Thornton et al., 1989)) this measurement is more sensitive to details of the junction scattering than the usual Hall or bend resistance measurements. Such an experiment would provide a rare opportunity to study chaotic scattering in the solid state, in a regime of unusual length scales and magnetic fields.

It is a pleasure to acknowledge stimulating discussions on this subject with the participants of the NATO ASI, in particular with M. Büttiker and M.L. Roukes.

REFERENCES

- Akera, H., and Ando, T., 1989, *Phys.Rev.B*, 39:5508.
 Avishai, Y., and Band, Y.B., 1989, *Phys.Rev.Lett.*, 62:2527.
 Baranger, H.U., and Stone, A.D., 1989, *Phys.Rev.Lett.*, 63:414;
 also in: "Science and Engineering of 1- and 0-Dimensional Semiconductors", S.P. Beaumont and C.M. Sotomayor-Torres, eds., Plenum, London, to be published.
 Beenakker, C.W.J., and Van Houten, H., 1988, *Phys.Rev.Lett.*, 60:2406;
 see also, Beenakker, C.W.J., Van Houten, H., and Van Wees, B.J., 1989, *Superlattices and Microstructures*, 5:127.

- Beenakker, C.W.J., and Van Houten, H., 1989a, *Phys.Rev.B*, 39:10445;
see also, Van Houten, H., and Beenakker, C.W.J., in: "Nanostructure Physics and Fabrication", M.A. Reed and W.P. Kirk, eds., Academic Press, New York, to be published.
- Beenakker, C.W.J., and Van Houten, H., 1989b, *Phys.Rev.Lett.*, 63:1857.
- Bleher, S., Ott, E., and Grebogi, C., 1989, *Phys.Rev.Lett.*, 63:919.
- Büttiker, M., 1986, *Phys.Rev.Lett.*, 57:1761; 1988, *IBM J.Res.Dev.*, 32:317.
- Büttiker, M., 1988, *Phys.Rev.B*, 38:9375.
- Chang, A.M., Timp, G., Howard, R.E., Behringer, R.E., Mankiewich, P.M., Cunningham, J.E., Chang, T.Y., and Chelluri, B., 1988, *Superlattices and Microstructures*, 4:515.
- Chang, A.M., Chang, T.Y., and Baranger, H.U., 1989, *Phys.Rev.Lett.*, 63:996.
- Ford, C.J.B., Thornton, T.J., Newbury, R., Pepper, M., Ahmed, H., Peacock, D.C., Ritchie, D.A., Frost, J.E.F., and Jones, G.A.C., 1988, *Phys.Rev.B*, 38:8518.
- Ford, C.J.B., Washburn, S., Büttiker, M., Knoedler, C.M., and Hong, J.M., 1989a, *Phys.Rev.Lett.*, 62:2724.
- Ford, C.J.B., Washburn, S., Büttiker, M., Knoedler, C.M., and Hong, J.M., 1989b, *Surf.Sci.*, to be published.
- Isawa, Y., 1989, preprint.
- Johnston, R., and Schweitzer, L., 1989, *J.Phys.Condensed Matter*, 1:4465.
- Kirzenow, G., 1989a, *Phys.Rev.Lett.*, 62:2993.
- Kirzenow, G., 1989b, *Solid State Comm.*, 71:469.
- Komiyama, S., and Hirai, H., 1989, preprint.
- Korzh, S.A., 1975, *Sov.Phys.JETP*, 41:70.
- Landauer, R., 1957, *IBM J.Res.Dev.*, 1:223; 1988, 32:306.
- MacDonald, D.K.C., 1949, *Nature*, 163:637;
see also, Pippard, A.B., 1989, "Magnetoresistance in Metals", Cambridge University Press, Cambridge.
- Molenkamp, L.W., Staring, A.A.M., Beenakker, C.W.J., Eppenga, R., Timmering, C.E., Williamson, J.G., Harmans, C.J.P.M., and Foxon, C.T., 1989, *Phys.Rev.B*, to be published.
- Peeters, F.M., 1988, *Phys.Rev.Lett.*, 61:589;
see also, 1989, *Superlattices and Microstructures*, 6:217.
- Peeters, F.M., 1989, in: "Science and Engineering of 1- and 0-Dimensional Semiconductors", S.P. Beaumont and C.M. Sotomayor-Torres, eds., Plenum, London, to be published.
- Phillips, J.C., 1988, *Phil.Mag.B*, 58:361.
- Ravenhall, D.G., Wyld, H.W., Schult, R.L., 1989, *Phys.Rev.Lett.*, 62:1780.
- Roukes, M.L., Scheier, A., Allen, S.J., Craighead, H.G., Ruthen, R.M., Beebe, E.D., and Harbison, J.P., 1987, *Phys.Rev.Lett.*, 59:3011.
- Roukes, M.L., Thornton, T.J., Scherer, A., Simmons, J.A., Van der Gaag, B.P., and Beebe, E.D., 1989, in: "Science and Engineering of 1- and 0-Dimensional Semiconductors", S.P. Beaumont and C.M. Sotomayor-Torres, eds., Plenum, London, to be published.
- Simmons, J.A., Tsui, D.C., and Weimann, G., 1988, *Surf.Sci.*, 196:81.
- Srivastava, V., 1989, *J.Phys.Condensed Matter*, 1:1919; 1:2025;
Srivastava, V., and Srinivasan, V., 1989, *J.Phys.Condensed Matter*, 1:3281.
- Takagaki, Y., Gamo, K., Namba, S., Ishida, S., Takaoka, S., Murase, K., Ishibashi, K., and Aoyagi, Y., 1988, *Solid State Comm.*, 68:1051.
- Takagaki, Y., Gamo, K., Namba, S., Takaoka, S., Murase, K., Ishida, S., Ishibashi, K., and Aoyagi, Y., 1989a, *Solid State Comm.*, 69:811.
- Takagaki, Y., Gamo, K., Namba, S., Takaoka, S., Murase, K., Ishida, S., 1989b, *Solid State Comm.*, 71:809.
- Thornton, T.J., Roukes, M.L., Scherer, A., Van Der Gaag, B., 1989, preprint.
- Timp, G., Chang, A.M., Mankiewich, P., Behringer, R., Cunningham, J.E., Chang, T.Y., and Howard, R.E., 1987, *Phys.Rev.Lett.*, 59:732.

- Timp, G., Baranger, H.U., deVegvar, P., Cunningham, J.E., Howard, R.E., Behringer, R., and Mankiewich, P.M., 1988, *Phys.Rev.Lett.*, 60:2081.
- Timp, G., Behringer, R., Samperc, S., Cunningham, J.E., and Howard, R.E., 1989, in: "Nanostructure Physics and Fabrication", M.A. Reed and W.P. Kirk, eds., Academic Press, New York, to be published.
- Tsoi, V.S., 1974, *JETP Lett.*, 19:70.
- Van Houten, H., Van Wees, B.J., Mooij, J.E., Beenakker, C.W.J., Williamson, J.G., and Foxon, C.T., 1988a, *Europhys.Lett.*, 5:721;
 Beenakker, C.W.J., Van Houten, H., and Van Wees, B.J., 1988, *Europhys.Lett.*, 7:359.
- Van Houten, H., Beenakker, C.W.J., Van Loosdrecht, P.H.M., Thornton, T.J., Ahmed, H., Pepper, M., Foxon, C.T., and Harris, J.J., 1988b, *Phys.Rev.B*, 37:8534.
- Van Houten, H., Beenakker, C.W.J., Williamson, J.G., Broekaaart, M.E.I., Van Loosdrecht, P.H.M., Van Wees, B.J., Mooij, J.E., Foxon, C.T., and Harris, J.J., 1989, *Phys.Rev.B*, 39:8556;
 for a review of electron focusing in a 2DEG, see: Beenakker, C.W.J., Van Houten, H., and Van Wees, B.J., 1989, *Festkörperprobleme*, 29:299.
- Van Wees, B.J., Van Houten, H., Beenakker, C.W.J., Williamson, J.G., Kouwenhoven, L.P., Van der Marck, D., and Foxon, C.T., 1988, *Phys.Rev.Lett.*, 60:848.
- Wharam, D.A., Thornton, T.J., Newbury, R., Pepper, M., Ahmed, H., Frost, J.E.F., Hasko, D.G., Peacock, D.C., Ritchie, D., and Jones, G.A.C., 1988, *J.Phys.C*, 21:L209.